PROCEEDINGS OF SPIE

SPIEDigitalLibrary.org/conference-proceedings-of-spie

Characterization and optimization of coupled-wave simulations for complex heterogeneous samples

Ruijiao Sun, Rohith Reddy, David Mayerich

Ruijiao Sun, Rohith Reddy, David Mayerich, "Characterization and optimization of coupled-wave simulations for complex heterogeneous samples," Proc. SPIE 11995, Physics and Simulation of Optoelectronic Devices XXX, 119950G (4 March 2022); doi: 10.1117/12.2609179



Event: SPIE OPTO, 2022, San Francisco, California, United States

Characterization and optimization of coupled-wave simulations for complex heterogeneous samples

Ruijiao Sun^a, Rohith Reddy^a, and David Mayerich^a

^aDepartment of Electrical and Computer Engineering, University of Houston, Houston, United States

ABSTRACT

Understanding the interactions between light and small samples at the diffraction limit is critical for solving inverse problems in microscopy. Several models for light and matter interactions have been proposed, including Born and Rytov approximations, Mie theory, T-matrix, Finite element methods, and coupled wave theory. Coupled wave approaches provide unique advantages for realistic samples by allowing refinement of the sample in the Fourier domain, where many realistic samples are considered sparse. However, this model still relies on computationally intensive operations as the sample and field resolution increases. In this paper, we develop an optimized open-source tool using established coupled-wave theory. This can be computationally efficient for realistic problems, since many practical samples are sparse in the Fourier domain. Then we analyze the computational complexity of the model and optimize the process.

Keywords: optical simulation, computational electromagnetics, Fourier Optics, Coupled Wave theory

1. INTRODUCTION

Understanding the interactions between light and samples at the diffraction limit is critical for solving inverse problems in microscopic and imaging. Several models for light-matter interactions have been proposed, including Born and Rytov approximations, Mie theory,¹ T-matrix,² and Finite element methods.³ However, these models have limitations when simulating heterogeneous, complex samples such as tissue. The Born approximation only accounts for a single scattering event, while Mie theory is limited to single spherical scatterers., while the T-matrix method is numerically unstable for highly elongated or flattened spheroids.⁴ The finite element method (FEM) divides the simulation domain into voxels, introducing a large number of boundary conditions that are computationally expensive to solve. Therefore, a general and optimized optical model is necessary for iterative calculations of inverse solutions,⁵ characterization of imaging systems with multiple interacting optical components,⁶ and fitting of all shapes of particles.

In this paper, we leverage an established coupled wave model⁷that incorporates multiple scattering by discretizing the spatial frequencies of a sample. This can be computationally efficient for realistic inverse problems, since many practical samples are sparse in the Fourier domain. In addition, this provides a physically practical method for controlling the sample complexity through a band limit. We show the simulation result for the electric field around three different sample shapes, such as a grating, cube, and sphere. We then profile the results and leverage high-efficiency libraries to improve computational speed.

2. THEORETICAL MODEL

A real optical system shown in 1(a) is composed of a single plane wave and an infinitely-layered sample consisting of homogeneous and heterogeneous layers. The incident plane wave travels down in the z direction and scatters at boundaries. In this paper, we only consider the "sandwich" sample shown as 1(b), which consists of 2 homogeneous layers at the top and the bottom and one heterogeneous layer composed of multiple sub-layers locates in the middle. This will likely allow for most real-world samples, however the technique is readily extended to multiple heterogeneous layers separated by homogeneous layers.

Consider a "sandwich" sample composed of 3 layers l = 0, 1, 2 with boundaries at z-axis coordinates $z^{(0)}$, $z^{(1)}$, and $z^{(2)}$. According to the theory of mid-infrared absorption,⁸ the first step is to decompose the layer property (permittivity), the plane wave and the wave propagation direction into N Fourier coefficients respectively so

Physics and Simulation of Optoelectronic Devices XXX, edited by Bernd Witzigmann, Marek Osiński, Yasuhiko Arakawa, Proc. of SPIE Vol. 11995, 119950G © 2022 SPIE · 0277-786X · doi: 10.1117/12.2609179

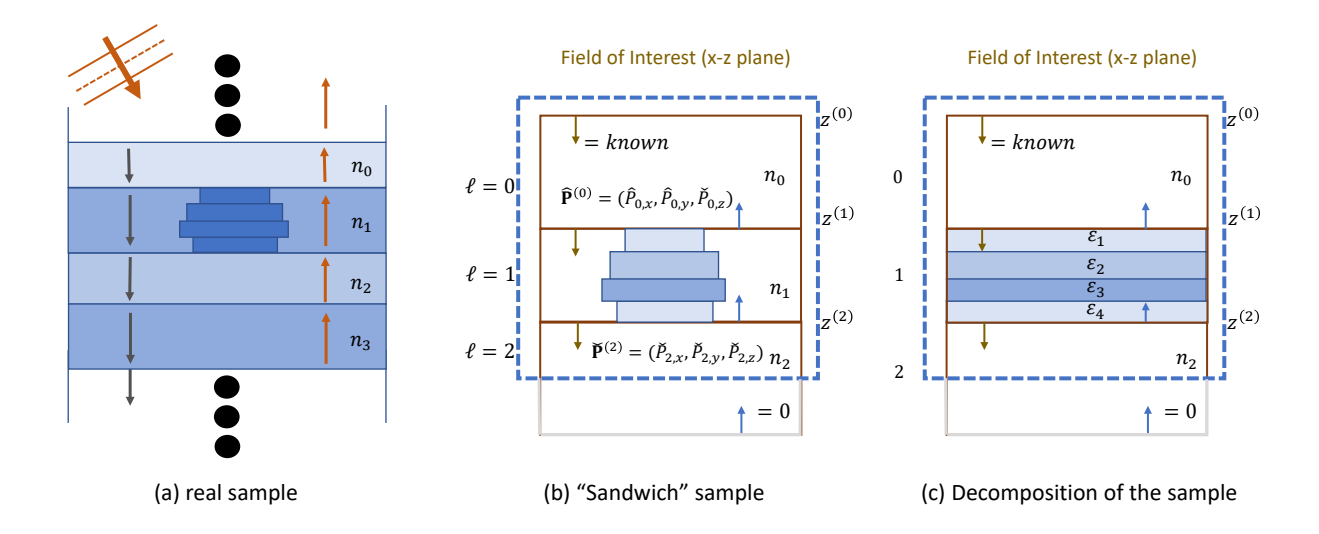


Figure 1. (a) is a real sample composed of multiple homogeneous or heterogeneous layers with different refractive indices incident by a single plane wave. Taking a simple "Sandwich" sample as an example in (b), we mark the refractive index n for each layer, which is the square root of the permittivity ε , the z position of each boundary z, and the electric field at each boundary P. Because of the necessity of the Fourier coefficients, we display one of the Fourier decomposed homogeneous layers in (c) whose permittivities are redistributed.

that each decomposed layer is homogeneous with specific wave component and propagation direction, shown in subsection 2.1. Next, we solve the electric field at the boundaries for the homogeneous layers by building a linear system, described in subsection 2.2 and then we derive the electric field at the boundaries for the heterogeneous layer from it. The last step is to use wave function to calculate the electric field for each point, shown in subsection 2.3.

2.1 Fourier Decomposition of the Heterogeneous Region

The heterogeneous sample region is characterized by upper and lower boundaries as well as the transverse structure defined by permittivity, $\varepsilon(x,y)$. For the decomposition of the permittivity, we group the slices along z axis which have the same distributions of the permittivity in x-y plane into multiple sub-layers (Shown as 1.c). We can index the sub-layers as $m, m \in [1, 2, ..., M]$, where $M \in [1, +\infty]$ is the number of the sub-layers. For a sub-layer m, the sample can be represented using the Fourier series

$$\epsilon(x, y, m) = \sum_{u = -U/2}^{U/2 - 1} \sum_{v = -V/2}^{V/2 - 1} \phi_{u, v}^{(m)}(z) \exp\left[i2\pi \left(\frac{ux}{X} + \frac{vy}{Y}\right)\right]$$
(1)

where $\epsilon \in \mathbb{C}$ is the square of the complex refractive index at position x, y located in sub-layer m, while $\phi^{(m)}$ are its corresponding Fourier coefficients. We will primarily be working with the reciprocal of the sample refractive index expressed using its spatial Fourier coefficients $\psi^{(m)}_{u,v}$:

$$\frac{1}{\epsilon(x,y,m)} = \sum_{u=-U/2}^{U/2-1} \sum_{v=-V/2}^{V/2-1} \psi_{u,v}^{(m)}(z) \exp\left[i2\pi \left(\frac{ux}{X} + \frac{vy}{Y}\right)\right]$$
(2)

For discretizing the wave propagation direction, the vector \mathbf{s} is the direction of propagation for a single plane wave. The electric field is made up of a set of N plane waves, with each representing a spatial frequency in the x-y plane. This set is discretized into propagation vectors $\mathbf{S} = \left[\mathbf{s}_{-N/2}, \cdots \mathbf{s}_{N/2}\right]$, where the index n corresponds to individual spatial frequencies:

$$\mathbf{s}_{n} = \begin{bmatrix} s_{x,n} \\ s_{y,n} \end{bmatrix} = \mathbf{s} + \frac{2\pi}{k} \begin{bmatrix} \frac{u}{X} \\ \frac{v}{Y} \end{bmatrix} = \mathbf{s}_{u,v}$$
 (3)

where X and Y are the size of the x - y plane, u and v is the indices in [0, X - 1] and [0, Y - 1] is the direction of the incident plane wave.

For the decomposed waves, the field vector for the downward-propagating transmitted plane wave at the upper boundary of layer-0 is a 3N-dimensional vector marked as $\hat{\mathbf{P}}^{(0)}(\mathbf{s})$, where $\hat{\mathbf{P}}^{(0)}(\mathbf{s}) = [\hat{\mathbf{P}}_x^{(0)}(\mathbf{s}), \hat{\mathbf{P}}_y^{(0)}(\mathbf{s}), \hat{\mathbf{P}}_z^{(0)}(\mathbf{s})]$ and $\hat{\mathbf{P}}_x^{(0)}(\mathbf{s}) = [\hat{\mathbf{P}}_{x,0}^{(0)}(\mathbf{s}), \hat{\mathbf{P}}_{x,1}^{(0)}(\mathbf{s}), \dots, \hat{\mathbf{P}}_{x,N-1}^{(0)}(\mathbf{s})]$. Correspondingly the field vector for the upward-propagating reflected plane wave at the lower boundary of layer-2 is $\check{\mathbf{P}}^{(2)}(\mathbf{s})$ with a dimension of 3N where $\check{\mathbf{P}}^{(2)}(\mathbf{s}) = [\check{\mathbf{P}}_x^{(2)}(\mathbf{s}), \check{\mathbf{P}}_y^{(2)}(\mathbf{s}), \check{\mathbf{P}}_z^{(2)}(\mathbf{s})]$ and $\check{\mathbf{P}}_x^{(2)}(\mathbf{s}) = [\check{\mathbf{P}}_{x,0}^{(2)}(\mathbf{s}), \dots, \check{\mathbf{P}}_{x,N-1}^{(2)}(\mathbf{s})]$. (1.b)

2.2 Electric Field at the Substrate Boundaries

The electric field at the homogeneous boundaries are represented by a 6N-dimensional vector, where 3N values represent reflected waves within the upper layer and 3N values represent transmitted waves for the bottom layer. The solution requires 6N linearly independent equations?? to solve the boundary fields. Gauss's Equation provides N linearly independent equations for the reflected wave in the upper layer and N linearly independent equations for the transmitted wave in the bottom layer. The other 4N equations are provided by Connection Equations, since the boundary conditions⁹ are not suitable for the heterogeneous layer.

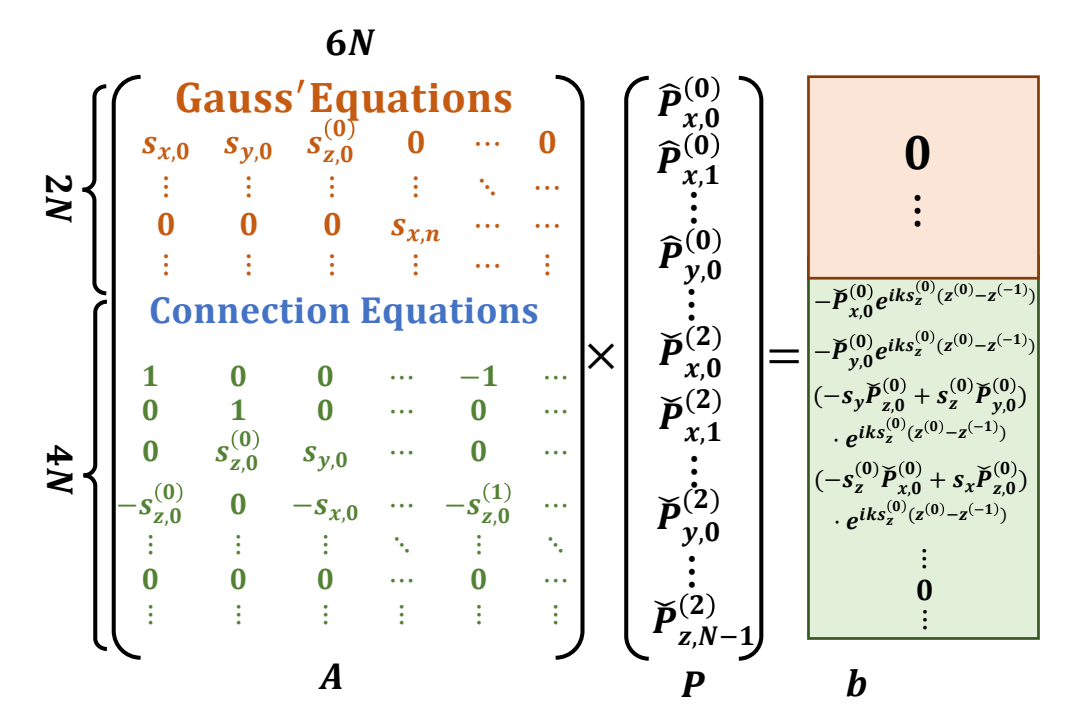


Figure 2. The electric field vector \mathbf{P} at the homogeneous boundaries is calculated by solving the linear system. For 6N linearly independent conditions, 2N are provided by Gauss' Equations (Equations 5 and 6) while the remaining 4N constraints are provided by the Connection Equations 7, 12, 8, 13, and 14.

2.2.1 Gauss's Law

We will utilize Maxwell's equations to dictate the transversality of the field in homogeneous layers. Gauss's equation $\nabla \cdot \mathbf{E}(\mathbf{r},t) = 0$ at the layer-l boundary in Fourier series can be written as

$$\frac{\partial \mathbf{P}}{\partial x} + \frac{\partial \mathbf{P}}{\partial y} + \frac{\partial \mathbf{P}}{\partial z} = \mathbf{s}^T \mathbf{P} = 0 \tag{4}$$

For this paper, we will have

$$s_x \check{\mathbf{P}}_x^{(0)}(\mathbf{s}) + s_y \check{\mathbf{P}}_y^{(0)}(\mathbf{s}) + s_z^{(0)} \check{\mathbf{P}}_z^{(0)}(\mathbf{s}) = 0$$
 (5)

$$s_x \hat{\mathbf{P}}_x^{(2)}(\mathbf{s}) + s_y \hat{\mathbf{P}}_y^{(2)}(\mathbf{s}) + s_z^{(2)} \hat{\mathbf{P}}_z^{(2)}(\mathbf{s}) = 0$$
(6)

where $[\check{\mathbf{P}}_x, \check{\mathbf{P}}_y, \check{\mathbf{P}}_z]^T$ is the field vector of $\check{\mathbf{P}}(\mathbf{s})$ and $\mathbf{s} = [s_x, s_y]^T$ and s_z are the z component of the propagation direction which is calculated by $s_z = \sqrt{n^2 - s_x^2 - s_y^2}$ where n is the refractive index (the square root of the permittivity ε) of the medium.

2.2.2 Connection Equations

The Connection Equations utilize the continuity of the transverse components of $\mathbf{E}(\mathbf{r},z)$ and $\mathbf{H}(\mathbf{r},z)$ across layer boundaries, which are also called boundary conditions for heterogeneous sample. We can easily write the Fourier coefficients of the electric field at the first boundary $z^{(1)}$ for layer-0 $\mathbf{P}^{z^{(1)}}=[\mathbf{P}_x^{z^{(1)}},\mathbf{P}_y^{z^{(1)}},\mathbf{P}_z^{z^{(1)}}]$, the x component for the n^{th} term of $\mathbf{P}^{z^{(1)}}$ is expanded below as

$$P_{x,n}^{z^{(1)}} = \check{P}_{x,n}^{(0)} \exp\left[iks_z \left(z^{(1)} - z^{(0)}\right)\right] + \hat{P}_{x,n}^{(0)} \tag{7}$$

Similarly, the x component for the n^{th} term of $\mathbf{P}^{z^{(2)}} = [\mathbf{P}_x^{z^{(1)}}, \mathbf{P}_y^{z^{(1)}}, \mathbf{P}_z^{z^{(1)}}]$ at the second boundary $z^{(2)}$ can be written as

$$P_{x,n}^{z^{(2)}} = \check{P}_{x,n}^{z^{(2)}} \tag{8}$$

To build the Fourier coefficients of the electric field at the boundaries for the heterogeneous layer, we utilize Faraday equation 9 and Ampère's circuit law 10 to build a 1^{st} order differential system that simplified as 27 for each sub-layer m. (The details about the mathematical derivation are attached in the auxiliary.)

$$\nabla \times \mathbf{E}(\mathbf{r}, z) = ik \sqrt{\frac{\mu_0}{\varepsilon_0}} \mathbf{H}(\mathbf{r}, z)$$
 (9)

$$\nabla \times \mathbf{H}(\mathbf{r}, z) = -ik\varepsilon(\mathbf{r})\sqrt{\frac{\varepsilon_0}{\mu_0}}\mathbf{E}(\mathbf{r}, z)$$
(10)

$$\begin{bmatrix} \frac{\partial \mathbf{P_x}}{\partial z} \\ \frac{\partial \mathbf{P_y}}{\partial z} \\ \frac{\partial \mathbf{Q_x}}{\partial z} \\ \frac{\partial \mathbf{Q_y}}{\partial z} \end{bmatrix} = ik\mathbf{D}^{(m)} \begin{bmatrix} \mathbf{P_x} \\ \mathbf{P_y} \\ \mathbf{Q_x} \\ \mathbf{Q_y} \end{bmatrix}$$
(11)

in which ${f P}$ and ${f Q}$ are the Fourier coefficients of the electric field ${f E}$ and the magnetic field ${f H}$ respectively.

After having $\mathbf{D}^{(m)}$ for sub-layer m, we do eigen-decomposition for it.

$$\mathbf{D}^{(m)} = \mathbf{G}^{(m)} \mathbf{\Gamma}^{(m)} \mathbf{G}^{(m)-1}$$

where diag $(\mathbf{\Gamma}^{(m)}) = [\gamma_1^{(m)}, -\gamma_1^{(m)}, \gamma_2^{(m)}, -\gamma_2^{(m)}, \cdots, \gamma_{2N}^{(m)}, -\gamma_{2N}^{(m)}]^T$ with all $\gamma_i^{(m)} \geq 0$ and $\mathbf{G}^{(m)}$ is expressed as a set of row vectors $\mathbf{G}^{(m)} = [\mathbf{g}_1^{(m)}, \mathbf{h}_1^{(m)}, ..., \mathbf{g}_{2N_F}^{(m)}, \mathbf{h}_{2N_F}^{(m)}]^T$. By substituting the eigen-decomposition result into 27, we can write down the representations of \mathbf{P}_x , \mathbf{P}_y , \mathbf{Q}_x , and \mathbf{Q}_y . We take an example of \mathbf{P}_x and represent $P_{x,n}^{z^{(1)}}$ and $P_{x,n}^{z^{(2)}}$ for the heterogeneous layer as

$$P_{x,n}^{z^{(1)}} = \sum_{j=1}^{2N} \left\{ \beta_j^{(1)} g_{j,n}^{(1)} + \hat{\beta}_j^{(1)} h_{j,n}^{(1)} \exp\left[-ik\gamma_j^{(1)} \left(z^{(\ell)} - z^{(m=1)}\right)\right] \right\}$$
(12)

$$P_{x,n}^{z^{(2)}} = \sum_{i=1}^{2N} \left\{ \beta_j^{(M)} g_{j,n}^{(M)} \exp\left[ik\gamma_j^{(M)} \left(z^{(m=M)} - z^{(m=M-1)}\right)\right] + \hat{\beta}_j^{(M)} h_{j,n}^{(M)} \right\}$$
(13)

where $\boldsymbol{\beta}^{(m)} = \left[\beta_j^{(m)}, \hat{\beta}_j^{(m)}\right]$ and $j \in [1, 2N]$ is a set of 4N unknown constants. The unknown $\boldsymbol{\beta}^{(m)}$ are the specific properties of sub-layer m.

For the heterogeneous layer consisting of more than 1 sub-layer, we build the Connection Equations for the *Heterogeneous/Heterogeneous Interface*.

$$\sum_{j=1}^{2N} \left\{ \beta_j^{(m-1)} g_{j,n}^{(m-1)} \exp\left[ik\gamma_j^{(m-1)} \left(z^{(m)} - z^{(m-1)}\right)\right] + \hat{\beta}_j^{(m-1)} h_{j,n}^{(m-1)} \right\} \\
= \sum_{j=1}^{2N} \left\{ \beta_j^{(m)} g_{j,n}^{(m)} + \hat{\beta}_j^{(m)} h_{j,n}^{(m)} \exp\left[-ik\gamma_j^{(m)} \left(z^{(m)} - z^{(m+1)}\right)\right] \right\}$$
(14)

Therefore we can build 4N linearly independent equations for \mathbf{P}_x , \mathbf{P}_y , \mathbf{Q}_x , and \mathbf{Q}_y that connects the electric field at the boundary $z^{(1)}$ with the electric field at the boundary $z^{(2)}$ by transferring the vector $\boldsymbol{\beta}$. This linear system that connects the two homogeneous layers can provide 4N equations to fill in the rest 4N rows for the coefficient matrix shown in Figure 2. Therefore we can solve the electric field at the boundaries for the two homogeneous layers by solving the coefficients matrix.

After solving the electric field at the homogeneous boundaries $[\hat{\mathbf{P}}^{(0)}, \check{\mathbf{P}}^{(0)}]$, we can utilize equations 7, 12, 8, 13, and 14 to calculate the vector $\boldsymbol{\beta}$.

2.3 Sample and Evaluate

The electric field within a homogeneous layer can be calculated by summing up the field vectors from the transmitted and the reflected waves:

$$\mathbf{E}(x,y,z) = \sum_{n=1}^{N} \left\{ \check{\mathbf{P}}^{(\ell)}(n) \exp\left[iks_{z}^{(\ell)}(n) \left(z - z^{(\ell-1)}\right)\right] + \hat{\mathbf{P}}^{(\ell)}(n) \exp\left[-iks_{z}^{(\ell)}(n) \left(z - z^{(\ell)}\right)\right] \right\} \times \exp\left[ik \left(s_{x}(n)x + s_{y}(n)y\right)\right]$$

$$(15)$$

where n_l is the refractive index of layer l and $z^{(\ell)}$ is the position of the boundary between layers l-1 and l. The complex exponential is used to propagate the plane waves from their locations at the boundary to the specified z coordinate. When the point is located in the heterogeneous layer, we can get the electric field from the eigen-decomposition result $G^{(m)}$, $\Gamma^{(m)}$ and the calculated $\beta^{(m)}$.

$$\mathbf{E}(x,y,z) = \sum_{j=1}^{2N} \left\{ \beta_j^{(m)} g_{j,n}^{(m)} \exp\left[ik\gamma_j^{(m)} \left(z - z^{(m-1)}\right)\right] + \hat{\beta}_j^{(m)} h_{j,n}^{(m)} \exp\left[-ik\gamma_j^{(m)} \left(z - z^{(m)}\right)\right] \right\}$$
(16)

3. SIMULATION RESULT

We simulated the optical field around samples interactively to validate the correctness of the model in this section. For our algorithm, the refractive index of the medium $n_0 = 1\mu m$ is considered as a constant for all layers, while the refractive index for the sphere is $n = 1.6\mu m$. The propagation direction of the incident wave is set as [0,0] meaning vertical to x - y plane. For display, we set the size of the whole region as $[40\mu m, 40\mu m, 40\mu m]$ while the center of the sample is located at [0,0,0]. The simulation result is shown in Figure 3 which is consistent with the result from Mie scattering.

Our model is generalized to fit different shapes of the samples. For examples, we set the wavelength to be $2\mu m$ and do simulation for a square sample and a grating sample shown in Figure 4 and 5.

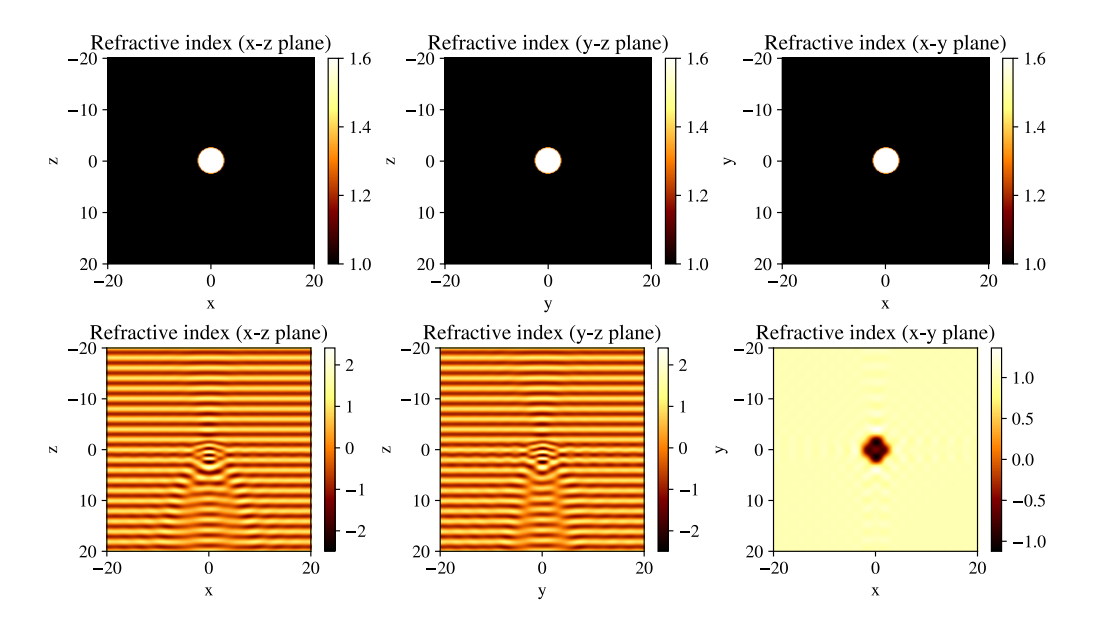


Figure 3. The wavelength for the incident plane wave is set as $2\mu m$. The propagation direction of the wave is vertical to x-y plane. The diameter of the spherical sample is $5\mu m$ with the center coordinate of (0,0,0). The area that we sampled the electric field has a size of $40\times 40\times 40\mu m^3$. In this figure, we show the electric field magnitude for x-z plane at y=0, the y-z plane at x=0, and the x-y plane at z=0 respectively.

4. COMPUTATIONAL ANALYSIS

Since the 3D modeling for electric field of millions of points is proved to be a time-consuming process, we do Big-O analysis in this section to figure out the computational complexity for each step.

4.1 Big-O analysis

We use X, Y, and Z as the number of the pixels along x, y, and z axes. N is the number of the Fourier coefficients. We can break the algorithm into a few steps and make Big-O analysis 10 for each step.

- 1. Calculate Fourier Coefficients The user specifies the heterogeneous component of the sample $\varepsilon(x,y,m)$ in terms of its relative permittivity (or the square of the complex refractive index). The ϕ and ψ coefficients for each $X \times Y$ sub-layer m are calculated using a Fourier Transform or FFT. This can be performed in O(MXYN) time.
- 2. Build the **D** matrices The matrix $\mathbf{D}^{(m)}$ shown in Equation 27 is assembled for each layer. Since $\mathbf{D} \in \mathbb{C}^{4N \times 4N}$ for each sub-layer, the whole process has a time complexity of $O(MN^2)$.
- 3. Eigen-decomposition of **D** The eigen-decomposition for each sub-layer $\mathbf{G}^{(m)}\mathbf{\Gamma}^{(m)}\mathbf{G}^{(m)-1} = \mathbf{D}^{(m)}$ can be performed with any standard algorithm. Since each matrix is $4N \times 4N$ and an eigen-decomposition has a time complexity of $O\left(n^3\right)$ for an $n \times n$ matrix, this operation for all the sub-layers requires $O\left(MN^3\right)$ time.
- 4. Solve for homogeneous Layers According to Figure 2, the first 6L-10 rows which only need to be filled by linear equations have a time complexity of O(N). The last 4L conditions need to be performed in O(MN) time resulted from the β connections for M sub-layers.
- 5. Solve β for heterogeneous Layers β is calculated by Equation 12, 13, and 14, which need a time complexity of O(MN) because β is for M sub-layers and N Fourier Coefficients.

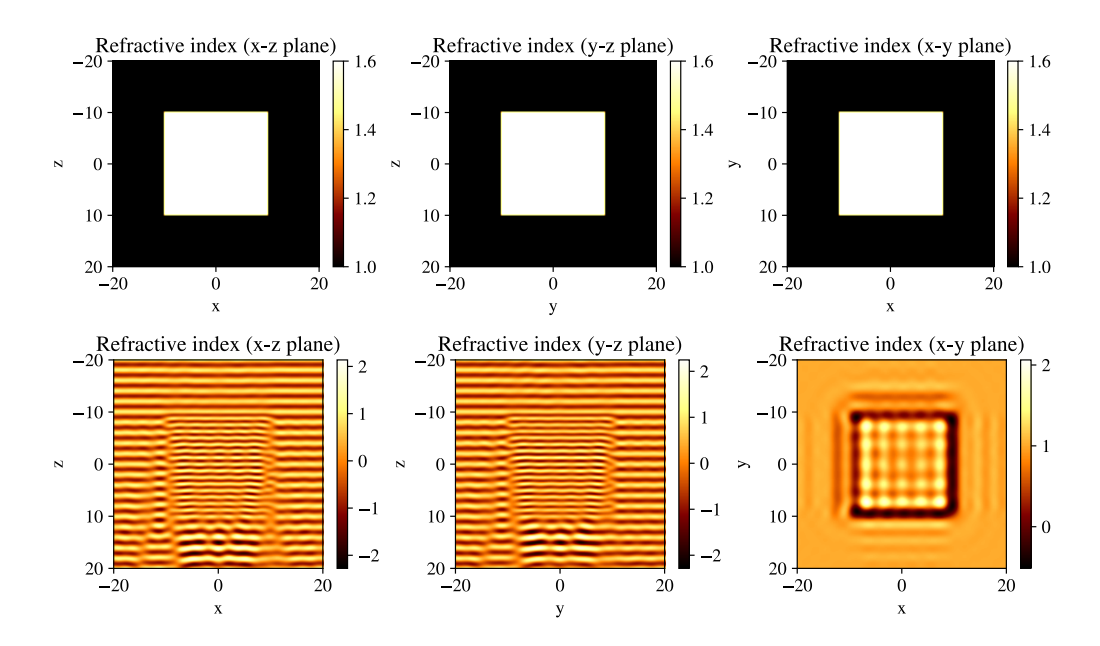


Figure 4. The wavelength for the incident plane wave is set as $2\mu m$ and the propagation direction of the wave is vertical to x-y plane. The refractive index for the square sample is 1.6 while the medium around the sample is 1.0. The size of the sample is $20 \times 20 \times 20 \mu m^3$ while the whole area is $40 \times 40 \times 40 \mu m^3$. The figure shows the electric field magnitude for x-z plane at y=0, the y-z plane at x=0, and the x-y plane at z=0.

6. Calculate the field for each point For the homogeneous layer, the calculation of the electric field for the whole region has a time complexity of O(XYZN). While for the heterogeneous layer, it needs a $O(max\{XYZN,MN^2\})$ time to calculate the electric field for each point.

4.2 Optimization for the algorithm

By analyzing the computational complexity for each step, we can use FFTPACK based Numpy. ifft and Numpy. ifft to do Fourier transformation instead of common Fourier transformation. ¹¹ In the meantime, we use LAPACK as the algorithm basis for doing eigen-decomposition for matrix D and solving linear functions to get boundary field vector P. Besides, we solve for vector β using BLAS. ¹²

For practical test, we simulate a singled-layered heterogeneous cube with a dimension of $100 \times 100 \times 100$, for which the number of Fourier coefficients is 24×24 . With the original configuration settings, the total collapsed time is 101 seconds, while it is 43 seconds after we use all the well-known and high-performance libraries mentioned before.

4.3 Further improvement

Another attracting feature is that several steps in this approach are highly amenable to inexpensive and accessible GPU parallelism.¹³ We are currently doing research on applying CUDA kernel to parallelize the most time-consuming sampling process by calculating electric field for each pixel independently. The support of CUDA will reduce the total execution time to be the level of one tenth.

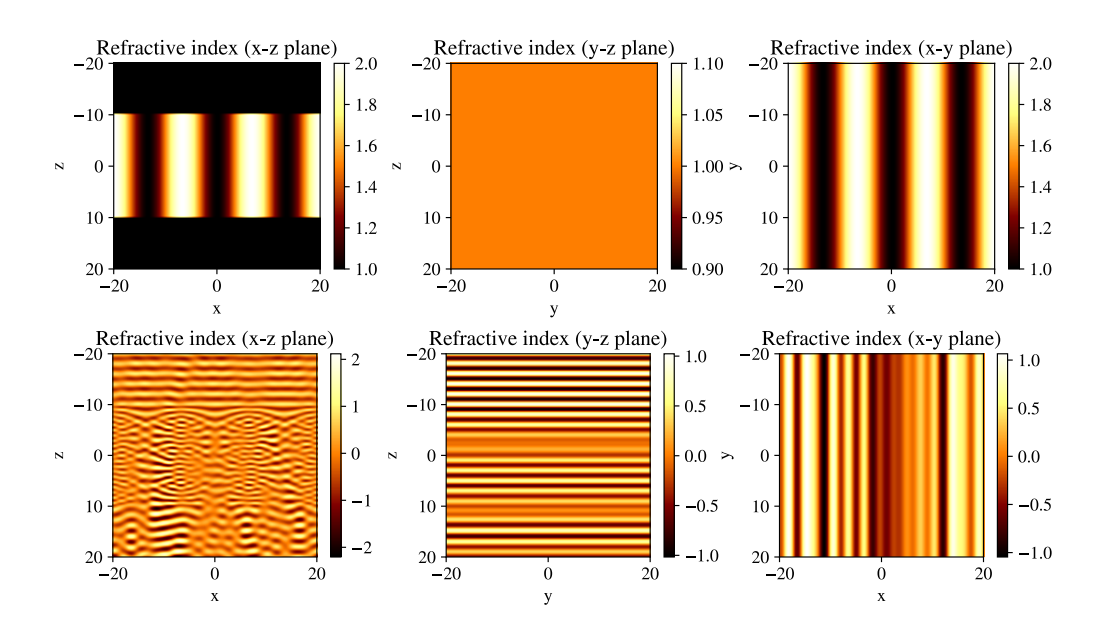


Figure 5. The wavelength for the incident plane wave is set as $2\mu m$ and the propagation direction of the wave is vertical to x-y plane. The refractive index for the grating sample is 1.6 while the medium is 1.0. The height of the sample is $20\mu m$ and it is infinite along y axis and z axis. Here we sample an area with size of $40 \times 40 \times 40 \mu m^3$. The electric field magnitude for x-z plane at y=0, the y-z plane at z=0, and the z=0 plane at z=0 is shown in this

APPENDIX A. BUILDING D

The evolution of the electric and magnetic fields with z can be expressed as equations 9 and 10. Applying the curl operator and expanding them gives:

$$\begin{bmatrix} \frac{\partial E_{z}(\mathbf{r},z)}{\partial y} - \frac{\partial E_{y}(\mathbf{r},z)}{\partial z} \\ \frac{\partial E_{x}(\mathbf{r},z)}{\partial z} - \frac{\partial E_{z}(\mathbf{r},z)}{\partial x} \\ \frac{\partial E_{y}(\mathbf{r},z)}{\partial x} - \frac{\partial E_{z}(\mathbf{r},z)}{\partial y} \end{bmatrix} = ik\sqrt{\frac{\mu_{0}}{\epsilon_{0}}} \begin{bmatrix} H_{x}(\mathbf{r},z) \\ H_{y}(\mathbf{r},z) \\ H_{z}(\mathbf{r},z) \end{bmatrix}$$
(17)

$$\begin{bmatrix} \frac{\partial H_{z}(\mathbf{r},z)}{\partial y} - \frac{\partial H_{y}(\mathbf{r},z)}{\partial z} \\ \frac{\partial H_{x}(\mathbf{r},z)}{\partial z} - \frac{\partial H_{z}(\mathbf{r},z)}{\partial x} \\ \frac{\partial H_{y}(\mathbf{r},z)}{\partial x} - \frac{\partial H_{x}(\mathbf{r},z)}{\partial y} \end{bmatrix} = -ik\varepsilon(\mathbf{r})\sqrt{\frac{\mu_{0}}{\varepsilon_{0}}} \begin{bmatrix} E_{x}(\mathbf{r},z) \\ E_{y}(\mathbf{r},z) \\ E_{z}(\mathbf{r},z) \end{bmatrix}$$
(18)

The electric field **E** and the magnetic fields **H** can be discretized (Equation 3) across spatial frequencies u, v as:

$$\mathbf{E}(\mathbf{r}, z) = \sum_{u} \sum_{v} \begin{bmatrix} P_{x}(\mathbf{s}_{u,v}, z) \\ P_{y}(\mathbf{s}_{u,v}, z) \\ P_{z}(\mathbf{s}_{u,v}, z) \end{bmatrix} \exp(ik\mathbf{s}_{u,v} \cdot \mathbf{r})$$

$$= \sum_{u} \sum_{v} \begin{bmatrix} P_{x}(\mathbf{s}_{u,v}, z) \\ P_{y}(\mathbf{s}_{u,v}, z) \\ P_{z}(\mathbf{s}_{u,v}, z) \\ P_{z}(\mathbf{s}_{u,v}, z) \end{bmatrix} \exp[iks_{x}(u, v)x + iks_{y}(u, v)y]$$
(19)

$$\mathbf{H}(\mathbf{r}, z) = \sqrt{\frac{\varepsilon_0}{\mu_0}} \sum_{u} \sum_{v} \begin{bmatrix} Q_x(\mathbf{s}_{u,v}, z) \\ Q_y(\mathbf{s}_{u,v}, z) \\ Q_z(\mathbf{s}_{u,v}, z) \end{bmatrix} \exp(ik\mathbf{s}_{u,v} \cdot \mathbf{r})$$

$$= \sqrt{\frac{\varepsilon_0}{\mu_0}} \sum_{u} \sum_{v} \begin{bmatrix} Q_x(\mathbf{s}_{u,v}, z) \\ Q_y(\mathbf{s}_{u,v}, z) \\ Q_z(\mathbf{s}_{u,v}, z) \end{bmatrix} \exp[iks_x(u, v)x + iks_y(u, v)y]$$
(20)

We will build a matrix of differential equations by separating the values from Equation 9 into individual components, discretizing them into spatial frequencies, and calculating their partial derivatives. We will use the second row of Equation 17 as an example. The differential equations will be the basis of the connection equations. First, we separate the values for $\nabla \times \mathbf{E}$:

$$\frac{\partial E_x(\mathbf{r}, z)}{\partial z} - \frac{\partial E_z(\mathbf{r}, z)}{\partial x} = ik\sqrt{\frac{\mu_0}{\epsilon_0}}H_y(\mathbf{r}, z)$$

We then use Equations 19 and 20 to decompose E and H into spatial frequencies:

$$\sum_{u} \sum_{v} \frac{\partial}{\partial z} P_{x}(\mathbf{s}_{u,v}, z) \exp\left[ik\left(s_{x}(u, v)x + s_{y}(u, v)y\right)\right] -$$

$$\sum_{u} \sum_{v} \frac{\partial}{\partial x} P_{z}(\mathbf{s}_{u,v}, z) \exp\left[ik\left(s_{x}(u, v)x + s_{y}(u, v)y\right)\right] =$$

$$\sum_{u} \sum_{v} ikQ_{y}(\mathbf{s}_{u,v}, z) \exp\left[ik\left(s_{x}(u, v)x + s_{y}(u, v)y\right)\right]$$

The partial derivatives can then be calculated for each spatial frequency u, v:

$$\frac{\partial P_x(\mathbf{s}_{u,v}, z)}{\partial z} - iks_x(u, v)P_z(\mathbf{s}_{u,v}, z) = ikQ_x(\mathbf{s}_{u,v}, z)$$

By continuing to substitute Equations 19 and 20 into Equation 17, separating components, and calculating partial derivatives, we can derive the following linearly independent equations for each spatial frequency u, v:

$$\frac{\partial P_x(\mathbf{s}_{u,v}, z)}{\partial z} = ikQ_y(\mathbf{s}_{u,v}, z) + iks_x(u, v)P_z(\mathbf{s}_{u,v}, z)$$
(21)

$$\frac{\partial P_y(\mathbf{s}_{u,v}, z)}{\partial z} = -ikQ_x(\mathbf{s}_{u,v}, z) + iks_y(u, v)P_z(\mathbf{s}_{u,v}, z)$$
(22)

$$Q_z(\mathbf{s}_{u,v}, z) = -s_y(u, v)P_x(\mathbf{s}_{u,v}, z) + s_x(u, v)P_y(\mathbf{s}_{u,v}, z)$$
(23)

We then perform a similar procedure for Ampere's equation. Substituting Equation 2, 19, and 20 into Equation 18 results in the following equations for each spatial frequency u, v:

$$\frac{\partial Q_x(\mathbf{s}_{u,v}, z)}{\partial z} = -ik \sum_{u'} \sum_{v'} \phi_{u-u',v-v'}^{(m)} P_y(\mathbf{s}_{u',v'}, z)
+ ik s_x(u, v) Q_z(\mathbf{s}_{u,v}, z)$$
(24)

$$\frac{\partial Q_y(\mathbf{s}_{u,v}, z)}{\partial z} = ik \sum_{u'} \sum_{v'} \phi_{u-u',v-v'}^{(m)} P_x(\mathbf{s}_{u',v'}, z)
+ ik s_y(u, v) Q_z(\mathbf{s}_{u,v}, z)$$
(25)

$$P_{z}(\mathbf{s}_{u,v}, z) = \psi^{(m)}(u, v) \otimes [s_{y}(u, v)Q_{x}(\mathbf{s}_{u,v}, z) - s_{x}(u, v)Q_{y}(\mathbf{s}_{u,v}, z)]$$

$$= \sum_{u'} \sum_{v'} \psi^{(m)}_{u-u', v-v'} s_{y}(u', v')Q_{x}(\mathbf{s}_{u', v'}, z)$$

$$- \sum_{u'} \sum_{v'} \psi^{(m)}_{u-u', v-v'} s_{x}(u', v')Q_{y}(\mathbf{s}_{u', v'}, z)$$
(26)

where the summations using u' and v' perform a convolution across all spatial frequencies.

Equations 21 through 26 are combined and concatenated to form the following linear system:

$$\begin{bmatrix} \frac{\partial \mathbf{P_x}}{\partial z} \\ \frac{\partial \mathbf{P_y}}{\partial z} \\ \frac{\partial \mathbf{Q_x}}{\partial z} \\ \frac{\partial \mathbf{Q_y}}{\partial z} \end{bmatrix} = ik \mathbf{D}^{(m)} \begin{bmatrix} \mathbf{P_x} \\ \mathbf{P_y} \\ \mathbf{Q_x} \\ \mathbf{Q_y} \end{bmatrix}$$
(27)

where the unknown N-dimensional sub-vectors $\mathbf{P_x}$ (from Equation 21), $\mathbf{P_y}$ (from Equation 22), $\mathbf{Q_x}$ (from Equation 24), and $\mathbf{Q_y}$ (from Equation 25) are assembled in the following format:

$$\mathbf{P_{x}} = \begin{bmatrix} P_{x} \left[\mathbf{s} \left(\frac{-U}{2}, \frac{-V}{2} \right), z \right] \\ P_{x} \left[\mathbf{s} \left(\frac{-U}{2} + 1, \frac{-V}{2} + 1 \right), z \right] \\ \vdots \\ P_{x} \left[\mathbf{s} \left(\frac{U}{2} - 1, \frac{V}{2} - 1 \right), z \right] \end{bmatrix}$$

$$(28)$$

and $\mathbf{D}^{(m)}$ is a known $4N \times 4N$ matrix that calculates the partial derivatives for sub-layer m.

For assembling the sub-layer matrix $D^{(m)}$, we substitute Equation 26 into Equation 21, Equation 22 and Equation 23 into Equation 24, Equation 25, we can get a new set of linear equations (shown as Figure 6).

$$\begin{split} \frac{\partial P_x(\mathbf{s}_{u,v},\partial z)}{\partial z} &= ikQ_y(\mathbf{s}_{u,v},z) \\ &+ iks_x(u,v)P_z(\mathbf{s}_{u,v},z) \\ &+ iks_x(u,v)\psi^{(m)}(u,v) \circledast s_y(u,v)Q_x(\mathbf{s}_{u,v},z) \\ &- iks_x(u,v)\psi^{(m)}(u,v) \circledast s_x(u,v)Q_y(\mathbf{s}_{u,v},z) \\ \frac{\partial P_y(\mathbf{s}_{u,v},\partial z)}{\partial z} &= -ikQ_x(\mathbf{s}_{u,v},z) + iks_y(u,v)P_z(\mathbf{s}_{u,v},z) \\ &= -ikQ_x(\mathbf{s}_{u,v},z) \\ &+ iks_y(u,v)\psi^{(m)}(u,v) \circledast s_y(u,v)Q_x(\mathbf{s}_{u,v},z) \\ &- iks_y(u,v)\psi^{(m)}(u,v) \circledast s_x(u,v)Q_y(\mathbf{s}_{u,v},z) \\ \frac{\partial Q_x(\mathbf{s}_{u,v},\partial z)}{\partial z} &= -ik\sum_{u'}\sum_{v'}\phi^{(m)}_{u-u',v-v'}P_y(\mathbf{s}_{u',v'},z) \\ &+ iks_x(u,v)Q_z(\mathbf{s}_{u,v},z) \\ &= -ik\phi^{(m)}_{u,v} \circledast P_y(\mathbf{s}_{u,v},z) \\ &+ iks_x(u,v)s_y(u,v)P_x(\mathbf{s}_{u,v},z) \\ \frac{\partial Q_y(\mathbf{s}_{u,v},\partial z)}{\partial z} &= ik\sum_{u'}\sum_{v'}\phi^{(m)}_{u-u',v-v'}P_x(\mathbf{s}_{u',v'},z) \\ &+ iks_y(u,v)Q_z(\mathbf{s}_{u,v},z) \\ &= ik\phi^{(m)}_{u,v} \circledast P_x(\mathbf{s}_{u,v},z) \\ &= ik\phi^{(m)}_{u,v} \circledast P_x(\mathbf{s}_{u,v},z) \\ &+ iks_y(u,v)S_y(u,v)P_x(\mathbf{s}_{u,v},z) \\ &+ iks_y(u,v)S_y(u,v)P_x(\mathbf{s}_{u,v},z) \\ &+ iks_y(u,v)S_y(u,v)P_y(\mathbf{s}_{u,v},z) \\ &+ iks_y(u,v)S_y(u,v)$$

where \circledast is a convolution operation:

$$\begin{aligned} \mathbf{a}(u,v) \circledast \mathbf{b}(u,v) &= \sum_{u'} \sum_{v'} \mathbf{a}(u-u',v-v') \mathbf{b}(u',v') = \\ &\begin{bmatrix} a \left[\left(u + \frac{U}{2} \right) \mod U, \left(v + \frac{V}{2} \right) \mod V \right] \\ a \left[\left(u + \frac{U}{2} - 1 \right) \mod U, \left(v + \frac{V}{2} \right) \mod V \right] \\ \vdots \\ a \left[\left(u - \frac{U}{2} + 1 \right) \mod U, \left(v + \frac{V}{2} \right) \mod V \right] \\ a \left[\left(u + \frac{U}{2} \right) \mod U, \left(v + \frac{V}{2} - 1 \right) \mod V \right] \\ \vdots \\ a \left[\left(u - \frac{U}{2} + 1 \right) \mod U, \left(v - \frac{V}{2} + 1 \right) \mod V \right] \end{bmatrix}^T \begin{bmatrix} b \left(-\frac{U}{2}, -\frac{V}{2} \right) \\ b \left(-\frac{U}{2}, -\frac{V}{2} \right) \\ \vdots \\ b \left(\frac{U}{2} - 1, -\frac{V}{2} \right) \\ \vdots \\ b \left(\frac{U}{2} - 1, \frac{V}{2} - 1 \right) \end{bmatrix} \end{aligned}$$

We provide examples of the internal structure of D by deriving two of its sub-matrix components (Figure 6).

$$\frac{1}{ik} \begin{bmatrix}
\frac{\partial P_x}{\partial z} \\
\frac{\partial P_y}{\partial z} \\
\frac{\partial Q_x}{\partial z} \\
\frac{\partial Q_y}{\partial z}
\end{bmatrix} = \begin{bmatrix}
0 & 0 & s_x \psi \otimes s_y & 1 - s_x \psi \otimes s_x \\
0 & 0 & -1 + s_y \psi \otimes s_y & -s_y \psi \otimes s_x \\
-s_x s_y & -\phi \otimes + s_x s_x & 0 & 0
\end{bmatrix} \begin{bmatrix}
P_x \\
P_y \\
Q_x \\
Q_y
\end{bmatrix}$$

Figure 6. Overview of the \mathbf{D} used to calculate the partial derivatives for each heterogeneous sub-layer m. We consider two sub-matrix components (black boxes) for detailed derivation.

First, consider the product $\mathbf{s}_x \boldsymbol{\psi} \circledast \mathbf{s}_y$, where the convolution is calculated by representing each component with sub-matrices in the linear system $\mathbf{S}_x \boldsymbol{\Psi} \mathbf{S}_y$ defined as:

$$\mathbf{S}_{x} = \operatorname{diag} \left\{ \begin{bmatrix} s_{x}(-\frac{U}{2}, -\frac{V}{2}) \\ s_{x}(-\frac{U}{2} + 1, -\frac{V}{2}) \\ \vdots \\ s_{x}(\frac{U}{2} - 1, \frac{V}{2} - 1) \end{bmatrix} \right\}$$

$$\mathbf{\Psi} = \begin{bmatrix} \psi_{0,0} & \psi_{-1,0} & \dots & \psi_{-U+1,0} \\ \psi_{1,0} & \psi_{0,0} & \dots & \psi_{-U+2,0} \\ \vdots \\ \psi_{U-1,V-1} & \psi_{U-2,0} & \dots & \psi_{0,0} \end{bmatrix}$$

$$\mathbf{S}_{y} = \operatorname{diag} \left\{ \begin{bmatrix} s_{y}(-\frac{U}{2}, -\frac{V}{2}) \\ s_{y}(-\frac{U}{2} + 1, -\frac{V}{2}) \\ \vdots \\ s_{y}(\frac{U}{2} - 1, \frac{V}{2} - 1) \end{bmatrix} \right\}$$

Next, consider the expression $-\phi \otimes +\mathbf{s}_x\mathbf{s}_x$ which will be represented by the linear system $-\Phi + \mathbf{S}_x\mathbf{S}_x$ where:

$$\mathbf{\Phi} = \begin{bmatrix} \phi_{0,0} & \phi_{-1,0} & \dots & \phi_{-U+1,0} \\ \phi_{1,0} & \phi_{0,0} & \dots & \phi_{-U+2,0} \\ \vdots & & & & \\ \phi_{U-1,V-1} & \phi_{U-2,0} & \dots & \phi_{0,0} \end{bmatrix}$$

in which the subscript of ψ and ϕ means the modulus of the current subscript. $\mathbf{s}_x, \mathbf{s}_y, \psi, \phi$ all have the dimensions of $N = U \times V$.

ACKNOWLEDGMENTS

This work has been supported in part by the National Institutes of Health / National Heart, Lung, and Blood Institute (NHLBI) #R01HL146745 and the National Science Foundation CAREER Award #1943455.

REFERENCES

- [1] Berisha, S., van Dijk, T., Bhargava, R., Carney, P. S., and Mayerich, D., "Bim-sim: Interactive simulation of broadband imaging using mie theory," *Frontiers in physics* 5, 5 (2017).
- [2] Egel, A., Eremin, Y., Wriedt, T., Theobald, D., Lemmer, U., and Gomard, G., "Extending the applicability of the t-matrix method to light scattering by flat particles on a substrate via truncation of sommerfeld integrals," *Journal of Quantitative Spectroscopy and Radiative Transfer* 202, 279–285 (2017).
- [3] Brenner, S. C., Scott, L. R., and Scott, L. R., [The mathematical theory of finite element methods], vol. 3, Springer (2008).
- [4] Waterman, P. C., "Symmetry, unitarity, and geometry in electromagnetic scattering," *Physical review* D **3**(4), 825 (1971).
- [5] Van Dijk, T., Mayerich, D., Carney, P. S., and Bhargava, R., "Recovery of absorption spectra from fourier transform infrared (ft-ir) microspectroscopic measurements of intact spheres," Applied Spectroscopy 67(5), 546–552 (2013).
- [6] Mayerich, D., Van Dijk, T., Walsh, M. J., Schulmerich, M. V., Carney, P. S., and Bhargava, R., "On the importance of image formation optics in the design of infrared spectroscopic imaging systems," Analyst 139(16), 4031–4036 (2014).
- [7] Marcuse, D., "Coupled-mode theory for anisotropic optical waveguides," The Bell System Technical Journal 54(6), 985–995 (1975).
- [8] Davis, B. J., Carney, P. S., and Bhargava, R., "Theory of mid-infrared absorption microspectroscopy: Ii. heterogeneous samples," *Analytical chemistry* 82(9), 3487–3499 (2010).
- [9] Davis, B. J., Carney, P. S., and Bhargava, R., "Theory of midinfrared absorption microspectroscopy: I. homogeneous samples," *Analytical chemistry* **82**(9), 3474–3486 (2010).
- [10] Heath, C. and Sitkin, S. B., "Big-b versus big-o: What is organizational about organizational behavior?," Journal of Organizational Behavior: The International Journal of Industrial, Occupational and Organizational Psychology and Behavior 22(1), 43–58 (2001).
- [11] Frigo, M. and Johnson, S. G., "The fastest fourier transform in the west. mit-lcs-tr-728," in [the Proceedings of the 1998 International Conference on Acoustics, Speech, and Signal Processing, ICASSP'98], Citeseer (1997).
- [12] Phillips, C., "The performance of the blas and lapack on a shared memory scalar multiprocessor," *Parallel computing* **17**(6-7), 751–761 (1991).
- [13] Keckler, S. W., Dally, W. J., Khailany, B., Garland, M., and Glasco, D., "Gpus and the future of parallel computing," *IEEE micro* **31**(5), 7–17 (2011).